PSFC/JA-03-21

Observations of Anomalous Momentum Transport in Alcator C-Mod Plasmas with No Momentum Input

J.E. Rice, W.D. Lee*, E.S. Marmar, P.T. Bonoli, R.S. Granetz,
M.J. Greenwald,
A.E. Hubbard, I.H. Hutchinson, J.H. Irby, Y. Lin, D. Mossessian,
J.A. Snipes,
S.M. Wolfe and S.J. Wukitch

September 2003

Plasma Science and Fusion Center
Massachusetts Institute of Technology
Cambridge, MA 02139 USA

*Archimedes Technology Group
San Diego, CA 92121 USA

This work was supported by the U.S. Department of Energy, Cooperative Grant No. DE-FC02-99ER54512. Reproduction, translation, publication, use and disposal, in whole or in part, by or for the United States government is permitted.

Submitted for publication to *Nuclear Fusion.*

Observations of Anomalous Momentum Transport in Alcator C-Mod Plasmas with No Momentum Input

J. E. Rice, W. D. Lee[†], E. S. Marmar, P. T. Bonoli, R. S. Granetz,
M. J. Greenwald, A. E. Hubbard, I. H. Hutchinson, J. H. Irby, Y. Lin,
D. Mossessian, J. A. Snipes, S. M. Wolfe and S. J. Wukitch
Plasma Science and Fusion Center, MIT, Cambridge, MA 02139-4307
[†]present address: *Archimedes Technology Group, San Diego, CA*

Abstract

Anomalous momentum transport has been observed in Alcator C-Mod tokamak plasmas. The time evolution of core impurity toroidal rotation velocity profiles has been measured with a tangentially viewing crystal x-ray spectrometer array. Following the L-mode to EDA (enhanced D_α) H-mode transition in both Ohmic and ICRF heated discharges, the ensuing co-current toroidal rotation velocity, which is generated in the absence of any external momentum source, is observed to propagate in from the edge plasma to the core with a time scale of order of the observed energy confinement time, but much less than the neo-classical momentum confinement time. The ensuing steady state toroidal rotation velocity profiles in EDA H-mode plasmas are relatively flat, with $V_\phi \sim 50$ km/s, and the momentum transport can be simulated with a simple diffusion model. Assuming the L-H transition produces an instantaneous edge source of toroidal torque (which disappears at the H- to L-mode transition), the momentum transport may be characterized by a diffusivity, with values of ~ 0.07 m^2/s during EDA H-mode and ~ 0.2 m^2/s in L-mode. These values are large compared to the calculated neo-classical momentum diffusivities, which are of order 0.003 m^2/s. Velocity profiles of ELM-free H-mode plasmas are centrally peaked (with $V_\phi(0)$ exceeding 100 km/s in some cases), which suggests the workings of an inward momentum pinch; the observed profiles are consistent with simulations including an edge inward convection velocity of ~ 10 m/s. In EDA H-mode discharges which develop internal transport barriers, the velocity profiles become hollow in the center, indicating the presence of a negative radial electric field well in the vicinity of the barrier foot. Upper single null diverted and inner wall limited L-mode discharges exhibit strong counter-current rotation (with $V_\phi(0) \sim -60$ km/s in some cases), which may be related to the observed higher H-mode power threshold in these configurations. For plasmas with locked modes, the toroidal rotation is observed to stop ($V_\phi \leq 5$ km/s).

I. Introduction

Rotation and velocity shear play important roles in the transition to high confinement mode (H-mode) [1, 2, 3, 4, 5], in the formation of internal transport barriers (ITBs) [6] and in suppression of resistive wall modes [7] in tokamak discharges. Compared to energy and particle transport, however, there has been considerably less effort addressing momentum transport. In a majority of tokamak plasmas, the toroidal rotation is generated externally by neutral beam injection. By measuring the rotation profiles from the associated beam diagnostics, and calculating the input torque profiles from the beam injection, momentum transport may be characterized [8, 9, 10, 11, 12, 13, 14, 15]. Momentum confinement is generally found to be anomalous, with a diffusivity, χ_ϕ, similar to the ion thermal conductivity, χ_i [8, 9, 10, 11, 12, 13, 14, 15], but much larger than the neo-classical diffusivity (viscosity). The reliability of this type of analysis relies on the accuracy of the input torque calculations, and the inherent assumption that there is no additional source of momentum when the plasma enters H-mode. Alcator C-Mod ICRF [16, 17] and Ohmic [16, 18, 19] H-mode discharges are found to have substantial spontaneous co-current toroidal impurity rotation (as high as 100 km/s, Mach number 0.3) in spite of the fact that there is no momentum input. Similar observations have been made on other devices such as JET[20, 21], COMPASS [22] and Tore Supra [23, 24, 25]. Several attempts to explain the observed rotation in C-Mod have been made, based on ICRF wave driven fast particle orbit shift mechanisms [26, 27, 28, 29], turbulence [30, 31] and sub-neo-classical [32] effects. The similarity of the rotation observed in ICRF and purely Ohmic plasmas suggests that it is not due to ICRF wave or fast particle effects. The prediction of reversal of the rotation direction with high magnetic field side (HFS) off-axis ICRF absorption [27, 29] has not been observed in the experiments [33]. For the turbulence driven theories [30, 31], the sign of the rotation is correct, but the magnitude cannot be tested because the turbulence fluctuation levels are not measured. The predictions of the rotation magnitude and direction from the sub-neo-classical theory agree with the measurements [32], but the calculated momentum diffusion time scale is two orders of magnitude longer than what is observed.

In order to gain a better understanding of the mechanism generating the rotation in the absence of an external source, and in general to characterize momentum transport, temporally resolved velocity profiles are needed. In the absence of neutral beam based diagnostics, a new tangentially viewing x-ray spectrometer array has been installed on Alcator C-Mod in order to provide this information. An outline of this paper is as follows: a brief description of the experiment and the spectrometer array is provided in II. Observed rotation profile evolution in H-mode plasmas is presented in III, along with modeling in IV. Rotation profiles for L-mode discharges in a variety of magnetic configurations are given in V with a discussion and conclusions in VI.

II. Experiment and Spectrometer Description

The rotation observations were obtained from the Alcator C-Mod tokamak, a compact (major radius 0.67 m, typical minor radius 0.21 m), high magnetic field ($B_T \leq 8$

T) device with strong shaping capabilities and all metal plasma facing components.

Auxilliary heating is available with 4 MW of ICRF heating power at 80 MHz, which is coupled to the plasma by 2 two-strap antennas. For the plasmas described here, the hydrogen minority heating was with $0 - \pi$ phasing, and there was no momentum input. An additional 4 MW of ICRF power are available at 78 MHz from a variable phase four-strap antenna; for the cases described here, this antenna was operated with $0 - \pi - 0 - \pi$ phasing, again with no momentum input. Previous off-axis toroidal rotation measurements from the doppler shifts of argon x-ray lines on Alcator C-Mod were from x-ray spectrometers with only a slight toroidal view [16], so only large rotation velocities could be seen, and only then with poor time resolution. The x-ray crystal spectrometer system has now been modified with three fully tangential views, vertically displaced to provide three points on the rotation profile. The spectrometer arrangement around the device is shown in Fig.1. The three spectrometers at

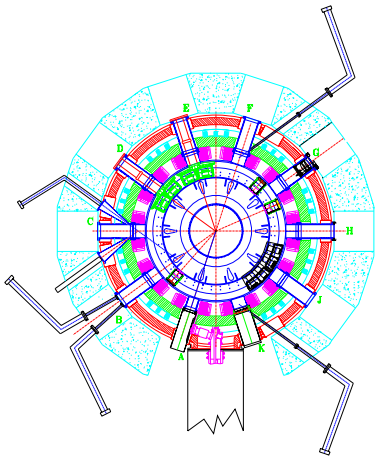

Figure 1: Top view of Alcator C-Mod with tangentially viewing x-ray spectrometers at C, F and K ports, and nearly perpendicular views at B port.

C, F and K ports have views which are tangent to R=0.685 m; the C port spectrometer is on the mid-plane while the F and K port spectrometers are vertically displaced by 0.09 and 0.18 m, respectively. The tangency points of these views superimposed on a (typical) magnetic flux plot are shown in Fig.2, along with the mapping to the outboard horizontal mid-plane, which demonstrates the profile coverage at r/a = 0.0, 0.3 and 0.6. Spatial resolution of these spectrometers is 1.5 cm. The central chord spectrometer observes the Ar^{17+} Ly_α doublet while the off-axis spectrometers monitor the Ar^{16+} forbidden line, z [16]. These three rotation measurements are augmented by the velocity of magnetic perturbations associated with sawtooth oscillations recorded with an array of fast pickup coils [18]. This provides rotation information at the q=1 surface,

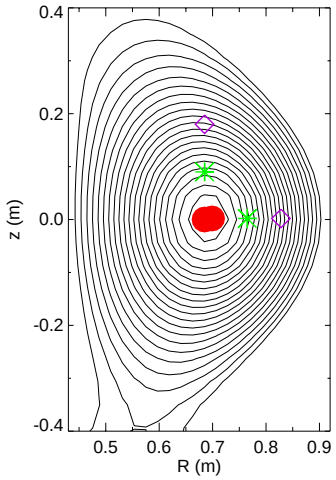

Figure 2: Side view of the tangency points of the three spectrometer views, superimposed on a magnetic flux surface plot. The mappings to the outboard horizontal mid-plane are also shown.

which is typically near r/a$\sim$0.2. Electron density profiles were determined by Thomson scattering and from the visible continuum using a high spatial resolution imaging CCD system. Electron temperature profiles were determined from Thomson scattering and from electron cyclotron emission (ECE). Magnetic flux surface reconstructions were provided from the EFIT [34] code.

III. Observed Rotation Profile Evolution in H-mode Plasmas

Previous measurements of toroidal rotation velocities in Alcator C-Mod H-mode plasmas, in the co-current direction and in the range of 20-120 km/s, have been largely restricted to the plasma center [16, 17, 33]. In going from L-mode to both Ohmic and ICRF H-mode, the change in the core rotation velocity was found to be proportional to the increase in the plasma stored energy normalized to the plasma current. Reversing the plasma current direction reverses the toroidal rotation direction. With the new tangential spectrometer array, a variety of different velocity profile shapes has been revealed. Shown in Fig.3 are the time histories of the (impurity) toroidal rotation velocities at three radii and the rotation of magnetic perturbations in pre- and post-cursors of sawtooth oscillations, for a 2.0 MW ICRF heated EDA H-mode [35] plasma. This 0.8 MA, 5.3 T discharge entered EDA H-mode at 0.655 s, as indicated by the drop in the D_α signal, with a subsequent increase in the plasma stored energy and toroidal rotation velocity [16, 17]. The velocity increase was first seen on the outermost spec-

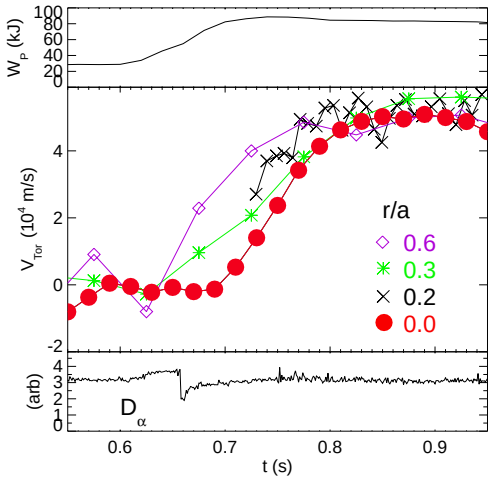

Figure 3: The plasma stored energy, impurity toroidal rotation velocity at three radii (red dots, green asterisks and purple diamonds for r/a = 0.0, 0.3 and 0.6, respectively), magnetic perturbation rotation ($\times$s) at the sawtooth inversion radius (r/a $\sim$ 0.2), and the edge D_α brightness for an ICRF heated EDA H-mode discharge.

trometer (r/a = 0.6), sequentially moving inward, suggesting an edge source of toroidal momentum which propagated in towards the center, with a time scale somewhat longer than $\tau_{\rm E}$, the energy confinement time. After about 150 ms (at 0.8 s), the rotation settled to a value of $\sim$50 km/s (in the co-current direction), with a flat profile. The fact that the rotation velocities for argon ions and m=1 perturbations are the same in steady state bolsters the argument that it is the bulk plasma rotation being measured [16, 18]. During this steady phase of the discharge, the central electron density was $2.8 \times 10^{20}/{\rm m}^3$ and the central electron temperature was 2.1 keV. Similar velocity profile evolution has been seen in purely Ohmic EDA H-mode plasmas. This time evolution and flat steady state rotation profile suggest that the momentum transport in EDA H-mode plasmas may be characterized by a purely diffusive process. The situation is different in ELM-free H-mode plasmas, as can be seen in Fig.4. This 0.8 MA, 4.6 T discharge entered ELM-free H-mode at 0.624 s, reverted to L-mode at 0.834 s, then re-entered ELM-free H-mode at 0.871 s. Following both L-H transitions, there was a rapid increase in the core rotation velocity and stored energy. In contrast to the EDA H-mode case, these rotation profiles are highly peaked (as in Fig.11 of Ref.[16]), reaching $\sim$70 km/s in the core (again in the absence of external momentum input) and $\sim$15 km/s at r/a=0.6. For such a profile to be sustained in steady state in the presence of momentum diffusion without a central momentum source requires there to be a mechanism of inward momentum transport up the velocity gradient, an inward momentum pinch [13]. During the first ELM-free period, the electron temperature was relatively constant at 1750 eV,

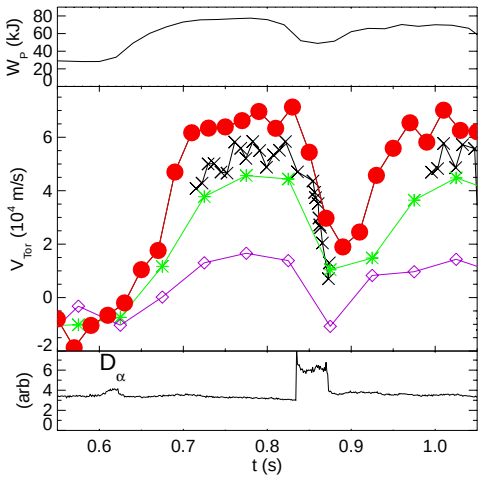

Figure 4: The plasma stored energy, impurity toroidal rotation velocity at three radii, magnetic perturbation rotation at the sawtooth inversion radius and the edge D $_\alpha$ brightness for an ICRF heated ELM-free H-mode discharge.

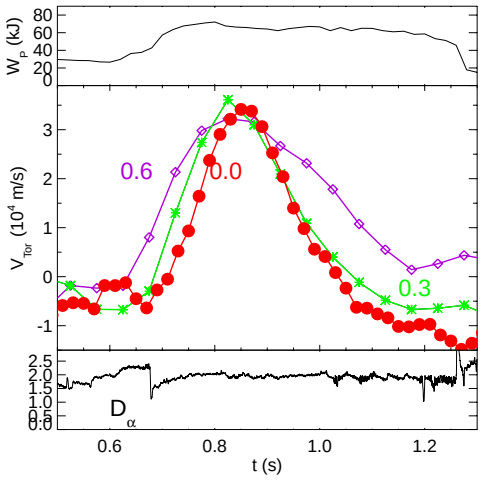

Figure 5: The plasma stored energy, impurity toroidal rotation velocity at three radii and the edge D$_\alpha$ brightness for an off-axis ICRF heated ITB discharge.

while the electron density rose continuously from 1.1 to 2.9 $\times$ 10^{20}/m^3, but maintaining a flat profile. Improved energy, particle and impurity confinement is a characteristic of ELM-free discharges; whether this momentum peaking is related is an open question. In contrast to these peaked rotation profiles are the hollow profiles which develop in internal transport barrier (ITB) plasmas. ITB discharges can be produced with off-axis ICRF heating [33, 36, 37], provided the resonance location is outside of r/a = 0.5, and that the plasma first enters EDA H-mode. These ITBs are characterized by a strong peaking of the core electron density which evolves in conjunction with a decrease and reversal of the core toroidal rotation velocity [33, 36]. Shown in Fig.5 are the rotation time histories for a 4.5 T, 0.8 MA EDA H-mode plasma produced with 2.2 MW of off-axis ICRF heating power at 80 MHz. Up until 0.85 s, this discharge exhibited the normal EDA H-mode rotation characteristics (Fig.3) with the rotation propagating in from the outside, and the profile becoming flat across most of the plasma. After 0.85 s, the core rotation inside r/a=0.5 (the location of the barrier foot) dropped and reversed direction (similar to Fig.7 of Ref.[33]) simultaneous with a strong peaking of the electron density profile also inside of r/a=0.5. The central electron density and temperature at 1.1 s were 6.0 $\times$ 10^{20}/m^3 and 1500 eV, respectively. The rotation at r/a=0.6, outside of the barrier foot, decreased more slowly and not so far, indicating a positive velocity gradient in the vicinity of the ITB foot. The radial electric field, $\mathrm{E_r}$, determined from the force balance equation and from calculations of the poloidal magnetic field, was found to be -8 kV/m at r/a=0.3 (inside of the ITB foot) and +8 kV/m at r/a=0.6 (outside of the foot), and a lower limit of the $\mathrm{E_r}$ gradient is $\sim$250 kV/m^2 at 1.1 s (see Fig.7 of [38]). A positive $\mathrm{E_r}$ gradient at the barrier foot is a common characteristic of ITB discharges.

The toroidal rotation velocity profiles for the previously described variety of H-mode plasmas are summarized in Fig.6. In the top frame are profiles from two different ELM-free H-mode discharges demonstrating the central peaking; the green points are from Fig.4 at 0.77 s. In the middle frame are profiles from two different EDA H-mode plasmas exhibiting flat shapes, at least out to r/a=0.6; the green points are from Fig.3 at 0.9 s and the red asterisks are from Fig.5 at 0.85 s. In the bottom frame is the hollow profile from the ITB discharge of Fig.5 at 1.07 s.

IV. Modeling of Rotation in H-mode Plasmas

The evolution of the toroidal rotation velocity profiles has been simulated using a simple source-free momentum transport model [39]

$$\frac{\partial}{\partial t}P + grad(-D_\phi \frac{\partial}{\partial r}P - \frac{v_c r}{a}P) = 0 \qquad (1)$$

with P = $n_i m_i V_\phi$, where a is the minor radius and where the momentum diffusivity, D_ϕ, and the momentum convection velocity, v_c, are free parameters to be determined. Positive v_c indicates inward convection. Subject to the boundary conditions of an edge rotation, V_0, which is present only during H-mode

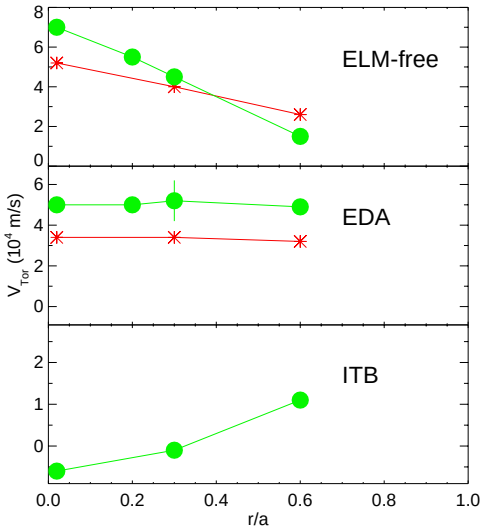

Figure 6: A comparison of toroidal rotation velocity profiles in two different ELM-free H-mode plasmas (top), two different EDA H-mode discharges (middle) and an ITB plasma (bottom).

$$V_\phi(a,t) = \begin{cases} 0, & t < t_{L\to H} \\ V_0, & t_{L\to H} \le t \le t_{H\to L} \\ 0, & t > t_{H\to L} \end{cases} \tag{2}$$

and with the assumptions (observed in the electrons) of a flat ion density profile and constant (spatially and temporally) D_ϕ and v_c, the toroidal rotation velocity, V_ϕ, profile evolution may be determined (in cylindrical coordinates) from a solution to

$$\frac{\partial}{\partial t}V_\phi - D_\phi\left[\frac{\partial^2}{\partial r^2}V_\phi + \left(\frac{1}{r} + \frac{v_c r}{aD_\phi}\right)\frac{\partial}{\partial r}V_\phi + \frac{2v_c}{aD_\phi}V_\phi\right] = 0 \tag{3}$$

via an expansion in confluent hypergeometric functions.

An example of a comparison of this model to the observed velocity time evolution in an EDA H-mode plasma similar to that presented in Fig.3 is shown in the top frame of Fig.7. The time of the L- to H-mode transition was 1.11 s. The three curves represent the simulated rotation velocities at the radii of the three spectrometer views. For this case, D_ϕ was spatially constant with a value of 0.05 m^2/s, and $v_c \approx 0$, which corresponds to a momentum confinement time, τ_ϕ, of 150 ms. This momentum diffusivity is much greater than the neo-classical viscosity [40], $\chi_\phi \sim \rho_i{}^2/\tau_{ii} \sim 0.003$ m^2/s for this case, and the momentum transport may be characterized as anomalous. The momentum diffusivity may also be determined for L-mode from the decay of the rotation velocity after the H- to L-mode transition at 1.53 s; D_ϕ for the L-mode portion of this discharge was 0.20 m^2/s, with $\tau_\phi \sim 35$ ms. From modeling of several ICRF and

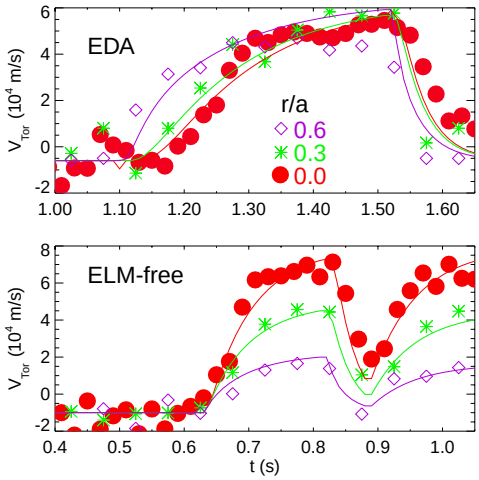

Figure 7: Comparison of model calculations (solid lines) with observed rotation time histories for an EDA H-mode plasma (top frame) and an ELM-free H-mode plasma (bottom frame).

Ohmic EDA H-mode plasmas, D_ϕ was found to be in the range from 0.05 to 0.10 m^2/s, with $v_c \approx 0$, and τ_ϕ in the range from 70-150 ms. The simulations for the ELM-free discharge from Fig.4 are shown in the bottom frame of Fig.7, which is on the same time scale as the top frame for comparison. In this instance D_ϕ was 0.40 m^2/s with v_c = 12 m/s, and $\tau_\phi \sim$70 ms. This value of the pinch velocity was necessary to match the quasi-steady peaked profile shape at 0.8 s (shown in Fig.6), with a 'peaking factor [41]', S $\equiv a v_c/2D_\phi$ = 3.2, along with the overall rise time of the rotation. From the rotation decay after the H- to L-mode transition (from 0.82-0.88 s), a value of $D_\phi \sim$0.25 m^2/s was determined. From the rotation decays in many discharges after the H- to L-mode transition (both EDA and ELM-free), D_ϕ for L-mode was determined to be in the range from 0.20-0.25 m^2/s, with v_c = 0.

The model of Eq.(3) cannot be strictly applied to the ITB case in Fig.5 because the electron (ion) and argon density profiles [36] were peaking in the core during the barrier evolution. However, along with the negative rotation velocity inside of the barrier foot, this implies a negative momentum density in the core, which would require an outward momentum convection in the core in the ITB phase.

V. Rotation in Ohmic L-mode Plasmas

In the two previous sections, the toroidal rotation velocity profiles in H-mode plasmas were characterized. L-mode discharges also display a wide variety of behavior,

although mostly in the counter-current direction. Earlier rotation observations of C-Mod discharges documented the counter-current rotation in Ohmic L-mode plasmas [42]. During the steady state phase of lower single null (LSN) diverted plasmas, the central rotation velocity was found to be in the range of -5 to -20 km/s [42, 16, 17]. (Here the minus sign indicates counter-current rotation.) This range in velocities is largely due to electron density variation. The magnetic configuration also has a strong effect on the magnitude of the counter-current rotation. This is demonstrated in Fig.8, which shows a comparison of two otherwise similar discharges which began with a LSN then switched to upper single null (USN). In the bottom frame is the distance be-

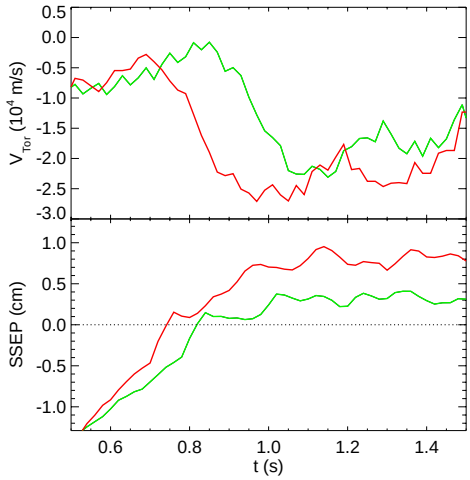

Figure 8: A comparison of the central rotation velocity (top) and the distance between the primary and secondary separatrices (bottom) for two successive discharges with LSN to USN switches.

tween the primary and secondary separatrices (SSEP), mapped to the midplane. When SSEP is negative, the plasma has a LSN, when SSEP is 0, the discharge has a double null and when SSEP is positive, there is an USN. The only difference between these two discharges was the timing of the USN transition. When each plasma switched to USN, there was a significant drop (an increase in the counter-current direction) in the central rotation velocity. These discharges both had the ion grad B drift downward. Presumably the change of ion orbits at the edge of the USN configuration led to a negative core E_r and stronger counter-current rotation. Strong counter-current rotation is also observed in the inner wall limited configuration. Shown in Fig.9 is a comparison of parameter time histories for similar successive discharges. In green is a LSN discharge and in red is an inner wall limited plasma. While the plasma parameters were similar, the inner wall limited discharge was rotating at -40 km/s. The electron density also has a strong effect on the observed rotation velocity in L-mode discharges. Shown in Fig.10 are electron density and toroidal rotation velocity profiles for two succes-

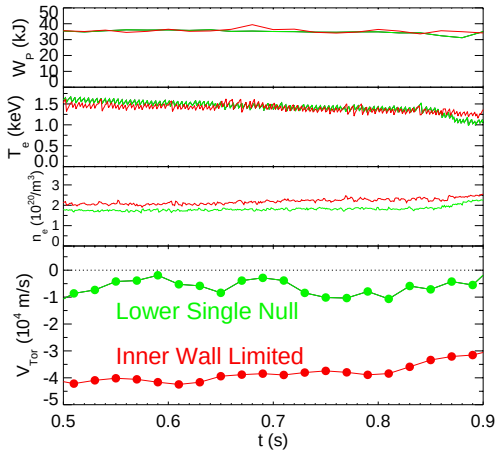

Figure 9: Parameter time histories from top to bottom of plasma stored energy, central electron temperature, central electron density and core toroidal rotation velocity for LSN (green) and inner wall limited (red) discharges.

sive 6.2 T, 0.8 MA inner wall limited discharges. The higher density plasma (green) had a flat velocity profile (~ -20 km/s) while the lower density discharge (red) had a strongly peaked profile with a central value of -55 km/s. The profile shown in red is nearly opposite to the peaked profiles in ELM-free H-modes shown in Fig.6 and is suggestive of a momentum pinch, albeit in the counter-current direction. This larger counter-current rotation at the center of lower density Ohmic L-mode discharges is in qualitative agreement with the predictions of neo-classical theory (Eq.56 of Ref.[43]).

One feature of C-Mod H-mode plasmas is the co-current toroidal rotation associated with the stored energy increase after the L-H transition. In fact there is a strong correlation between rotation velocity and H-factor (Fig.10 of Ref.[16]). It may be that for limited and USN diverted discharges, which exhibit strong counter-current rotation, the rotation increase which ensues after ICRF injection is not enough to be significantly co-current, so the plasma remains in L-mode. This notion is demonstrated in Fig.11, which shows a comparison between parameters in two similar discharges, one with a double null (DN) and the other an USN. The target parameters and ICRF power (1.5 MW) were the same in both of these 5.4 T, 0.8 MA deuterium plasmas. The DN discharge (green, with SSEP near 0) entered EDA H-mode at 0.85 s with the usual increases in stored energy, electron density and toroidal rotation velocity (which was strongly co-current). The USN discharge (red, with SSEP positive) exhibited an increase in the rotation velocity, but since the target plasma was rotating at -40 km/s, the final level was barely co-current. If a large enough edge velocity gradient is required to be present to make the transition, apparently it was not enough for this plasma to enter

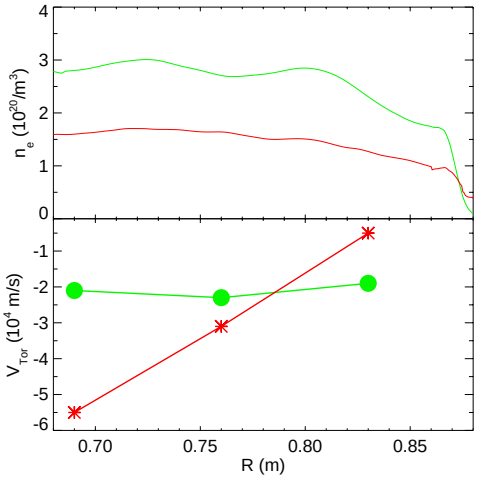

Figure 10: Electron density (top) and rotation velocity (bottom) profiles for two inner wall limited discharges.

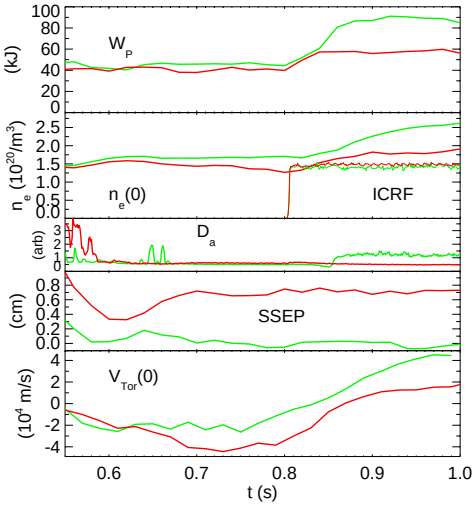

Figure 11: Parameter time histories, from top to bottom, of the plasma stored energy, central electron density (and ICRF power waveform), D_α brightness, SSEP and central toroidal rotation velocity for double null (green) and upper single null (red) discharges.

H-mode. The strong counter-current rotation observed in USN and limited discharges may be related to the higher power threshold for plasmas in these configurations to make the L-H transition.

In discharges with locked modes, the toroidal rotation has been observed to stop [44, 45]. Similar behavior has also been seen in C-Mod plasmas. Shown in Fig.12 are parameter time histories for an Ohmic L-mode discharge which developed a locked mode at ∼0.96 s. The locked mode formation was accompanied by a drop in stored

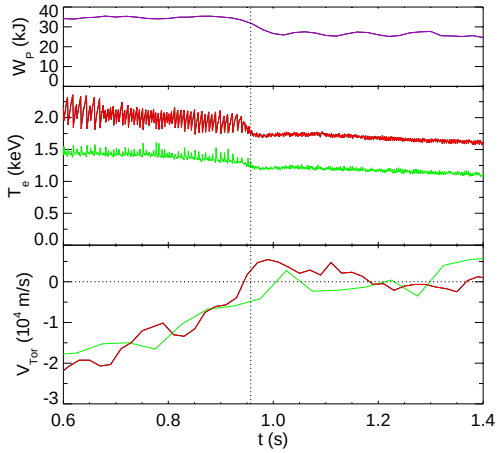

Figure 12: The plasma stored energy (top frame), electron temperature (middle frame) at the center (red) and r/a∼0.3 (green) and the toroidal rotation velocity (bottom frame) at r/a=0.0 (red) and r/a=0.3 (green) for a discharge which developed a locked mode.

energy and electron temperature, disappearance of sawtooth oscillations and a braking of the toroidal rotation velocity. These modes occur in C-Mod plasmas with low density and high plasma current. In this particular case, all of these events occured at about the same time. Another example of a locked mode plasma is shown in Fig.13. In this case the central rotation halted before the disappearance of the sawtooth oscillations. The rotation stopped in less than 20 ms, which interestingly is shorter than the L-mode momentum confinement time. The evolution of most C-Mod locked modes includes a double sawtooth event (1.15 s) followed by an increase in the sawtooth period (after 1.20 s) and eventual loss of sawtooth oscillations (1.37 s). In this case the drop in stored energy and the halt in the rotation were correlated with the sawtooth period increase. Part of the temperature profile was eroded at this time as the q=1 surface moved inward, as seen in the inversion of sawteeth at r/a∼0.3 (green).

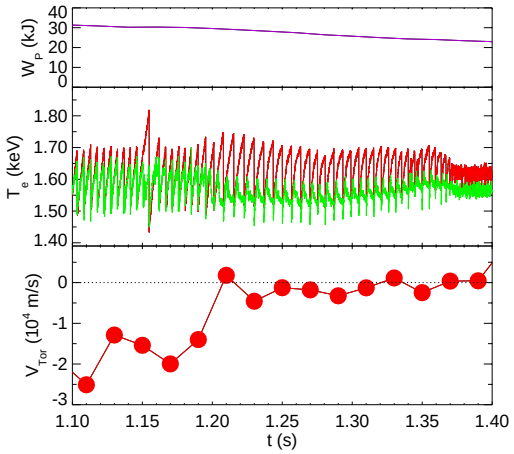

Figure 13: A locked mode plasma (same legend as Fig.12).

VI. Discussion and Conclusions

In the progression from L-mode to EDA H-mode to ELM-free H-mode to ITB discharges, the particle diffusivity steadily drops (particle confinement increases), approaching neo-classical levels in the core in ITB plasmas. Electron density profiles in L-mode discharges are centrally peaked (with no edge pedestal), EDA H-mode plasmas have temporally and spatially constant electron density profiles inside of the edge pedestal, ELM-free H-mode plasmas exhibit steadily rising electron density profiles which maintain a flat shape and ITB discharges show a central peaking of the density profile [33, 36] consistent with the neo-classical Ware pinch velocity. The same sequence of impurity confinement may be characterized as highly anomalous in L-mode, with an impurity diffusivity $D_I \sim 0.5$ m^2/s ($\tau_I \sim$ 15-25 ms) and $D_I \sim$ 0.1-0.3 m^2/s in EDA H-mode with $\tau_I \sim$ 50-150 ms [46]. For ELM-free H-mode plasmas, the impurity confinement is long ($\tau_I \sim 1$ s) with reduced D_I (~ 0.05 m^2/s) and substantial inward convection (10-100 m/s) at the edge [46]. In ITB discharges there is strong core impurity accumulation [36] with D_I (~ 0.02 m^2/s) and v_I ($\sim$ 100 ms inward), close to the neo-classical values in the core plasma. Energy confinement exhibits a somewhat similar progression with χ_{eff} dropping from $\sim$1 m^2/s in L-mode, to $\sim$0.5 m^2/s in H-mode [35] and then as far as $\sim$0.1 m^2/s (near the neo-classical level) in the core plasma during ITB [36] operation. Momentum confinement demonstrates some similarities in behavior; there is a decrease in the momentum diffusivity from 0.20-0.25 m^2/s in L-mode to the range 0.05-0.10 m^2/s in EDA H-mode. Also, in ELM-free H-mode there is a strong momentum pinch, with $v_c \sim$10 m/s, analogous to the observations of impurity transport. With such a large value of the inward pinch, an increase in the

Mode	D	D_I	D_ϕ	χ_{eff}
L	0.15	0.5	0.2-0.25	1.0
EDA		0.1-0.3	0.05-0.1	0.5
ELM-free		0.05	0.4	0.5
ITB	0.01	0.02	0.05?	0.1

Table 1: The particle, impurity, momentum and thermal diffusivities in m^2/s.

Mode	v	v_I	v_c
L		0	0
EDA		10	0
ELM-free		10-100	10
ITB	0.1	100	-2?

Table 2: The particle, impurity and momentum convection velocities in m/s.

momentum diffusivity was required to match the profile shape and velocity rise time scale. In ITB discharges, particle, impurity and energy confinement may be characterized by transport coefficients with values similar to neo-classical levels in the core. For these discharges, however, the momentum seems to be expelled from the plasma center, rather than having increased confinement. From a fit to the hollow ITB velocity profile in Fig.6, a value of -2.3 is found for the peaking factor S. From the decay time of the core velocity in the ITB phase, D_ϕ is determined [41] to be $\sim$0.05 m^2/s, if the ITB foot radius is used, and v_c is ~ -2 m/s. The reason that the momentum transport in ITB discharges doesn't follow the behavior of particle and energy confinement may be because these plasmas have a negative E_r well in the core, and may be influenced by the fact that momentum is an odd moment of the distribution function, with directionality. The momentum transport in ITB discharges does not seem to be tied to energy confinement. A similar difference in behavior is seen in discharges with locked modes, where the energy confinement is slightly degraded, but the momentum is lost from the plasma [44]. Representative values for the particle, impurity, momentum and thermal diffusivities in the various confinement modes are summarized in Table 1, with the convection velocities (here, positive values indicate inward) in Table 2.

The momentum transport in C-Mod has been found to be anomalous, with momentum diffusivities much larger than neo-classical levels. The cause of the toroidal rotation, which appears to propagate in from the plasma edge, and is generated in the absence of a momentum source, remains unexplained.

L-mode plasmas generally exhibit counter-current rotation. Inner wall limited and upper single null discharges have stronger counter-current rotation than lower single or double null plasmas, which may be related to their observed higher H-mode power threshold. For L-mode plasmas which develop locked modes, the rotation is seen to halt.

V. Acknowledgements

The authors thank J. Terry for D_α measurements, S. Scott for useful discussions and the Alcator C-Mod operations and ICRF groups for expert running of the tokamak. Work supported at MIT by DoE Contract No. DE-FC02-99ER54512.

References

[1] K.C.Shaing and E.C.Crume, Phys. Rev. Lett. **63** (1989) 2369.

[2] H.Biglari et al., Phys. Fluids **B2** (1990) 1.

[3] R.J.Groebner et al., Phys. Rev. Lett. **64** (1990) 3015.

[4] K.Ida et al., Phys. Rev. Lett. **65** (1990) 1364.

[5] P.W.Terry, Rev. Mod. Phys. **72** (2000) 109.

[6] K.Burrell, Phys. Plasmas **4** (1997) 1499.

[7] E.J.Strait et al., Phys. Rev. Lett. **74** (1994) 2483.

[8] S.Suckewer et al., Nucl. Fusion **21** (1981) 1301.

[9] K.H.Burrell et al., Nucl. Fusion **28** (1988) 3.

[10] S.D.Scott et al., Phys. Rev. Lett **64** (1990) 531.

[11] A.Kallenbach et al., Plasma Phys. Contr. Fusion **33** (1991) 595.

[12] N.Asakura et al., Nucl. Fusion **33** (1993) 1165.

[13] K.Nagashima et al., Nucl. Fusion **34** (1994) 449.

[14] K.-D.Zastrow et al., Nucl. Fusion **38** (1998) 257.

[15] J.S.deGrassie et al., Nucl. Fusion **43** (2003) 142.

[16] J.E.Rice et al., Nucl. Fusion **38** (1998) 75.

[17] J.E.Rice et al., Nucl. Fusion **39** (1999) 1175.

[18] I.H.Hutchinson et al., Phys. Rev. Lett. **84** (2000) 3330.

[19] J.E.Rice et al., Phys. Plasmas **7** (2000) 1825.

[20] L.-G.Eriksson et al., Plasma Phys. Contr. Fusion **39** (1997) 27.

[21] J.-M.Noterdaeme et al., Nucl. Fusion **43** (2003) 274.

[22] I.H. Coffey, R. Barnsley, F.P. Keenan *et al.*, in Proceedings of the 11th Colloquium on UV and X-ray Spectroscopy of Astrophysical and Laboratory Plasmas, Nagoya, Japan, 1995, p.431, Frontiers Science Series No.15 (Editors: K. Yamashita and T. Watanabe), Universal Academy Press, Tokyo, Japan, 1996

[23] G.T.Hoang et al., Nucl. Fusion **40** (1999) 913.

[24] L.-G.Eriksson et al., Nucl. Fusion **41** (2001) 91.

[25] S.Assas et al., 'Toroidal plasma rotation in ICRF heated Tore Supra discharges', 30th European Physical Society Conference on Plasma Physics and Controlled Fusion, St. Petersburg, Russia, 7-11 July 2003, ECA Vol. **27A** P-1.138

[26] C.S.Chang et al., Phys. Plasmas **6** (1999) 1969.

[27] F.W.Perkins et al., Phys. Plasmas **8** (2001) 2181.

[28] V.S.Chan et al., Phys. Plasmas **9** (2002) 501.

[29] L.-G.Eriksson and F.Porcelli, Nucl. Fusion **42** (2002) 959.

[30] K.C.Shaing, Phys. Rev. Lett. **86** (2001) 640.

[31] B.Coppi, Nucl. Fusion **42** (2002) 1.

[32] A.L.Rogister et al., Nucl. Fusion **42** (2002) 1144.

[33] J.E.Rice et al., Nucl. Fusion **41** (2001) 277.

[34] L.L.Lao et al., Nucl. Fusion **25** (1985) 1611.

[35] M.Greenwald et al., Nucl. Fusion **37** (1997) 793.

[36] J.E.Rice et al., Nucl. Fusion **42** (2002) 510.

[37] S.J.Wukitch et al., Phys. Plasmas **9** (2002) 2149.

[38] J.E.Rice et al., Nucl. Fusion **43** (2003) 781.

[39] W.D.Lee et al., submitted to Phys. Rev. Lett. (2003).

[40] F.L.Hinton and S.K.Wong, Phys. Fluids **28** (1985) 3088.

[41] F.H.Seguin et al., Phys. Rev. Lett. **51** (1983) 455.

[42] J.E.Rice et al., Nucl. Fusion **37** (1997) 421.

[43] Y.B.Kim et al., Phys. Fluids **B3** (1991) 2050.

[44] J.A.Snipes et al., Nucl. Fusion **28** (1988) 1085.

[45] R.J.Buttery et al., Nucl. Fusion **39** (1999) 1827.

[46] J.E.Rice et al., Phys. Plasmas **4** (1997) 1605.